Journal of Power Sources 264 (2014) 100–107

Contents lists available at ScienceDirect

Journal of Power Sources

journal homepage: www.elsevier.com/locate/jpowsour

# Influence of temperature and upper cut-off voltage on the formation of lithium-ion cells

Florian German [a], Andreas Hintennach [a], Annette LaCroix [a], Denny Thiemig [b], Steffen Oswald [c], Frieder Scheiba [d], Michael J. Hoffmann [d], Helmut Ehrenberg [d,*]

[a] Daimler AG, Mercedesstrasse 137, D-70327 Stuttgart, Germany
[b] Li-Tec Battery GmbH, Am Wiesengrund 7, D-01917 Kamenz, Germany
[c] IFW Dresden, Institute for Complex Materials, Helmholtzstrasse 20, D-01069 Dresden, Germany
[d] Karlsruhe Institute of Technology (KIT), Institute for Applied Materials (IAM), Kaiserstrasse 12, D-76131 Karlsruhe, Germany

## HIGHLIGHTS

- The influence of temperature on the formation of Li-ion cells was investigated.
- Increasing temperature decreases formation loss due to enhanced Li-diffusion in NMC.
- Increasing formation temperature worsens cell performance of graphite anode.
- The influences of both anode and cathode on a full cell were examined.
- The components of the solid electrolyte interphase on the anode were determined.

## ARTICLE INFO

*Article history:*
Received 11 March 2014
Received in revised form
10 April 2014
Accepted 15 April 2014
Available online 26 April 2014

*Keywords:*
Solid electrolyte interphase
Lithium-ion battery
Formation
Electrode
Raman microscopy

## ABSTRACT

The influences of temperature on the formation losses and subsequent electrical performance of $Li_x(Ni_{1/3}Co_{1/3}Mn_{1/3})_yO_2$ (NCM)/graphite lithium-ion cells were investigated. It was shown that the total capacity loss during formation of a full cell at 25 °C consists of losses on the positive and negative electrode to about one half each. The losses of the negative electrode (ca. 10%) are due to solid electrolyte interphase (SEI) formation on graphite but are masked by the losses of the positive side (ca. 20%) which are mainly caused by a kinetic inhibition of NCM and are theoretically reversible when the cell is discharged to very low potentials. The total loss of a full cell fits with the loss of the positive electrode. With increased temperature the ratio of losses on positive and negative electrode decreases as the diffusion coefficient of lithium in NCM increases. In total, an elevated formation temperature leads to increased irreversible losses on both electrodes and significantly lower cell performance of graphite. The upper cut-off voltage has an influence on the positive electrode formation losses in a reversible manner. The constituents of the SEI identified via the combination of XPS and FTIR are mainly $RCH_2OCO_2Li$, RCOOLi and LiF for the outer SEI and mainly $Li_2CO_3$, $Li_2O$ and LiF for the inner SEI.



## 1. Introduction

Lithium-ion batteries have been used since the early 1990s as power sources for portable devices like cell phones, laptop computers or digital cameras. Due to their high energy and power densities, reliability, long cycle life and safety, they also became attractive for hybrid electric vehicles, full electric vehicles and stationary energy storage.

Many commercially available lithium-ion batteries consist of a graphite negative electrode and a lithium metal oxide positive electrode, e.g. $Li_{1+x}(Ni_{1/3}Co_{1/3}Mn_{1/3})_{1-x}O_2$ (NCM).

It is generally known that the initial charge of a graphite negative electrode leads to irreversible loss of lithium (irreversible capacity). This is due to the formation of the so-called solid electrolyte interphase (SEI), a passivating layer on the surface of graphite, which is formed via the reaction of electrolyte components with lithium particularly during the initial charge before intercalation [1–3]. The SEI protects the electrolyte from further decomposition and the negative electrode from co-intercalation of solvent molecules into graphite and thus its exfoliation. The performance, aging

* Corresponding author. Tel.: +49 721 608 47915.
*E-mail address:* helmut.ehrenberg@kit.edu (H. Ehrenberg).

http://dx.doi.org/10.1016/j.jpowsour.2014.04.071
0378-7753/

and safety of a lithium-ion cell are strongly affected by the properties of the SEI, therefore it is indispensable to assure a sufficient SEI formation [4–7]. For this reason the first charge and if required also further charge–discharge cycles, in total called the formation, must undergo a defined process with well selected parameters. Influences of temperature [8–12], current [13–15], voltage profile [16–18] and the used materials (type of graphite and electrolyte composition) [19,20] on the composition and morphology and therefore functional properties of the SEI have been investigated. With the use of ethylene carbonate (EC)-based electrolytes, typical species found in the SEI are lithium alkyl carbonates ($ROCO_2Li$), lithium alkoxides (ROLi), lithium alkyl carboxylates (RCOOLi), lithium carbonate ($Li_2CO_3$), lithium oxide ($Li_2O$), lithium hydroxide (LiOH) and lithium fluoride (LiF) [21–24].

Also NCM positive electrodes show poor first-cycle efficiency. There are reports on formation losses due to surface film formation [25] or other parasitic electrochemical reactions as a function of particle surface area [26]. In contrast Kang et al. showed that the assumed physical loss of lithium in conventional voltage range is only a kinetic behavior and can be fully recovered below 1.5 V by applying a deep discharge [27,28].

However, in most commercial lithium-ion cells both graphite negative electrode and metal oxide positive electrode are present and it is not trivial to assign the initial losses and further aging effects to the different electrodes. In this work, the charging conditions and materials (graphite and NCM) of a commercial pouch cell were applied to three-electrode half cells containing either graphite or NCM as the working electrode to figure out the roles of the two electrodes in matters of formation losses and aging impact in full cells. For this procedure the formation was executed at different temperatures to understand its effect on the SEI formation and subsequent cell performance. Also the influence of the upper cut-off voltage on the formation was investigated.

The characterization of the SEI was performed with X-ray photoelectron spectroscopy (XPS), attenuated total reflection Fourier transform infrared spectroscopy (ATR-FTIR) and Raman spectroscopy.

## 2. Experimental

Lithium-ion pouch cells ("full cells") from Li-Tec Battery (HEA50, 50 Ah) consisting of a graphite negative electrode, $Li_x(Ni_{1/3}Co_{1/3}Mn_{1/3})_yO_2$ (NCM) positive electrode, polymer separator and an ethylene carbonate based organic electrolyte with lithium hexafluorophosphate as conducting salt were used in this study. The "half cells" (electrochemical measurements of electrodes vs. metallic lithium) were assembled using three-electrode test cells (EL-Cell, type ECC-Ref) with the electrode (graphite or NCM) to be investigated as working electrode, lithium metal (Alfa Aesar, purity 99.9%) as counter and reference electrodes, a glass microfiber mat (Whatman, type GF/D) soaked with electrolyte as separator. For some experiments the test cells were configured with both graphite and NCM electrodes as well. Before transferred into the argon-filled glovebox ($H_2O$ and $O_2 < 1$ ppm) for half-cell assembly the active materials and separators were dried under vacuum at 130 °C for at least 12 h and subsequently hermetically sealed. The electrochemical tests with pouch cells were carried out using a multiple cell tester (Digatron, MCT Series). The test cells were investigated by the use of potentiostats (Gamry, type Reference 600). For temperature control, temperature chambers (Vötsch, different types) were used.

The formation was performed for all cells in a similar way. The C-rate is based on the capacity of the positive electrode (limiting electrode) of the pouch cell after formation, and was downscaled using the area of the electrode for the test cells. The terms charge and discharge always refer to a full cell. Charging of a graphite half-cell is therefore the intercalation of lithium into graphite. Charging NCM means the extraction of lithium out of the NCM host lattice. First the cells were charged with a current of C/10 (1C is the current needed to charge a cell within 1 h to its nominal capacity) for 10 h, and then discharged to 3.0 V (full cell), 3.0 V vs. $Li^+$/Li (NCM) or 1.5 V vs. $Li^+$/Li (graphite), respectively. The time-limited charge has been chosen to achieve a comparable capacity in all cells since the exact potentials vs. $Li^+$/Li of the electrodes in the full cell are not known. In the case of discharging a time-limited process would be useless in respect to the differences in formation losses considered here. In the subsequent cycles potential limits were used for both charge and discharge processes to observe the capacity fade due to the increase of the internal resistivity. For the pouch cells limits of 4.2 and 3.0 V and a current of 3C were chosen. NCM was cycled between 3.0 and 4.2 V vs. $Li^+$/Li and graphite between 0.04 and 1.5 V vs. $Li^+$/Li, both with a current of C/2, respectively. The different currents were chosen according to the different internal resistivities.

For analysis of the SEI the pouch cells (50% state-of-charge) were opened in a glovebox and appropriate negative electrode samples were cut out. The samples were washed with diethyl carbonate (DEC) for various times and vacuum-dried in the antechamber for 1 h before hermetically sealed for transport or directly measured in the glovebox.

The ATR-FTIR analysis was carried out in the glovebox using a Tensor 27 system (Bruker) together with a DuraSamplIR II (Smiths Detection) containing a three-reflection DuraDisk. A resolution of 4 $cm^{-1}$ and a scan number of 16 were used.

XPS measurements were conducted with a PHI 5600 CI (Physical Electronics) spectrometer with a pass energy of 29 eV and an analysis area of 800 μm in diameter. Monochromatic Al-$K_\alpha$ excitation (350 W) and a low-energy electron neutralizer were used. To avoid air contact of the samples, the system was equipped with a transfer chamber. Sputter depths profiling was done using $Ar^+$ ions (3.5 keV, scan size 3 × 3 mm) with conditions leading to a 0.4 nm $min^{-1}$ sputter rate, determined for a $SiO_2$ reference.

For the Raman spectroscopy the electrodes were placed in air-tight spectroscopic cells equipped with glass optical windows. The measurements were carried out using a LabRAM HR (Horiba Jobin Yvon) with a 633 nm HeNe laser (about 11 mW), an 100× objective, a motorized *xy*-stage and an analysis area of 3 × 4 μm (wobble scan technique, 15 s integration time).

## 3. Results and discussion

### 3.1. Formation

Fig. 1a shows the formation curves at 25 °C for a commercial pouch cell, an NCM half-cell and a graphite half-cell. The differences in capacity between charging and discharging curves are the formation losses. Obviously, the losses of both NCM and the full cell exceed those of graphite. In Fig. 1b these losses are displayed for different formation temperatures, respectively. The losses of the full cell and that of the NCM half-cell are about the same at one formation temperature (25–45 °C). The small deviations can be related to the chosen lower cut-off voltages of 3.0 V for both potentials NCM vs. $Li^+$/Li and NCM vs. graphite (Fig. 1a). The significant higher losses at 15 °C for the NCM half-cell compared to the full cell could be due to the inner resistivity which plays a more dominant role at low temperatures for the half-cell geometry. Apparently, the formation losses of graphite electrodes increase with temperature while those of NCM decrease. The temperature dependency of the irreversible charge losses of the commercial cell

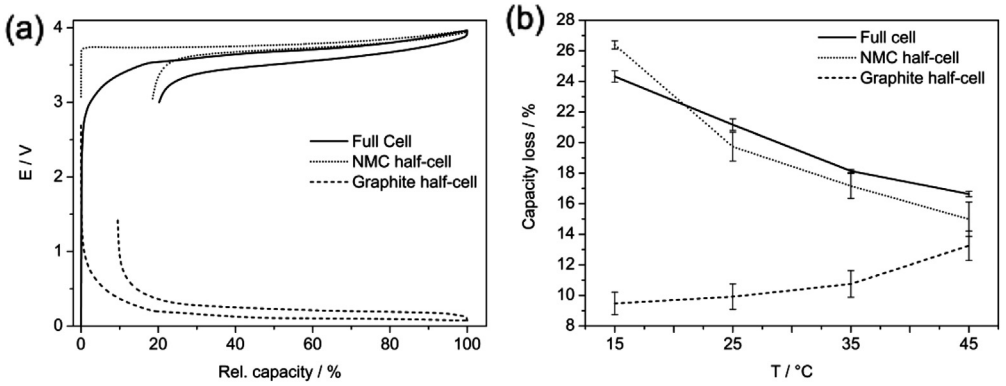


**Fig. 1.** (a) Formation curves of different cells at 25 °C. All cells were charged with C/10 for 10 h, and then discharged with C/2 to 3.0 V (full cell), 3.0 V vs. $Li^+$/Li (NCM) or 1.5 V vs. $Li^+$/Li (graphite). (b) Formation losses of these cells for different temperatures. At least 4 cells were used per test.

is therefore strongly affected by the NCM positive electrode, whilst influences of the negative electrode are not visible. The behavior of graphite is also found in literature [8,11,12] and is correlated with SEI formation [8,9]. With increasing formation temperature both the irreversible losses and the SEI thickness increase. An elevated temperature leads to a greater extent of structural defects as pores and flaws within the SEI, and also the exfoliation tendency of graphite increases. The reverse trend for both NCM and pouch cells indicates a kinetic effect with improved diffusion at elevated temperature. This behavior will be discussed later. The high standard deviations for the losses of half cells can be attributed to its different assembly compared to the commercial cells. This discrepancy also affects the cell performance as it will be shown in the following experiments.

### 3.2. Cell performance

The pouch cells and half cells were cycled after formation at room temperature (23 °C). For pouch cells a cycle number of 1400 was chosen, and for the half cells a number of 20. The results are displayed in Fig. 2. For the entire range of cycling the coulombic efficiencies for the half cells and full cells were clearly above 99 and 99.9%, respectively. For all types of cells the decrease of capacity is due to an increase of the inner resistivity whereby the potential limits are reached earlier. Exemplary the progresses of the relative resistivities of the pouch cells during cycling are displayed in Fig. 2d. These resistivities ($\Delta U/I$) were obtained by applying discharge pulses of 2C for 18 s at 50% SOC, where $\Delta U$ is given by the voltage change from 50% SOC until the end of the pulse.

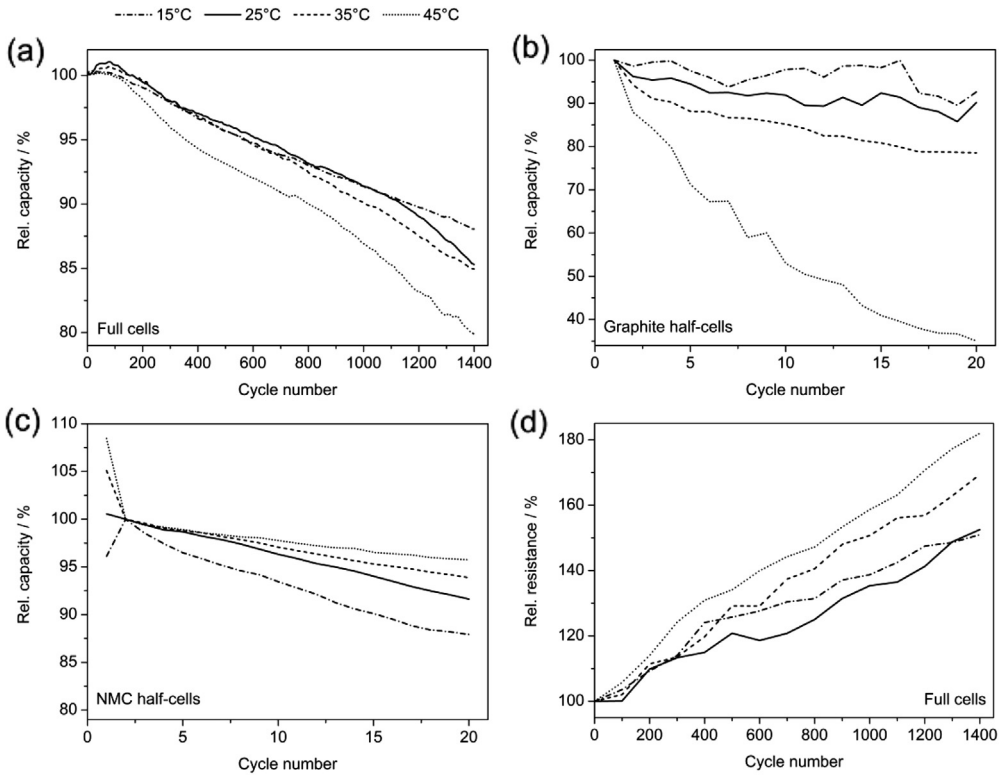


**Fig. 2.** (a–c) Plots of relative capacity against cycle number obtained from cycling at room temperature of (a) pouch cells (3C between 3.0 and 4.2 V), (b) graphite half cells (C/2 between 0.04 and 1.5 V vs. $Li^+$/Li) and (c) NCM half cells (C/2 between 3.0 and 4.2 V vs. $Li^+$/Li). (d) Progress of the relative discharge resistivity (2C pulse for 18 s at 50% SOC) during cycling of pouch cells displayed in (a). The specified temperatures refer to the temperatures during formation, while cycling was always performed at 23 °C.

Apparently, the electrical performance for the commercial pouch cell decreases with formation temperature. Especially a temperature of 45 °C seems to deteriorate capacity retention noticeably. The capacity fade originates from an increase of the inner resistivity due to aging impacts like SEI formation or structural degradation of the electrodes. Right after formation the resistivities of all pouch cells were almost identical and were defined as 100% relative resistivity (Fig. 2d). With increasing formation temperature the slope of the resistivity curve increases. To understand the influences on this behavior the results of the half-cell measurements will be discussed in the following.

The cyclability for NCM half cells slightly improves with an increased formation temperature. While the "absent" formation losses of cells with formation temperatures above 25 °C show up during their first cycle at room temperature the 15 °C cell regains a part of its capacity when the temperature rises to room temperature. This shows that the capacity of the NCM material is strongly temperature dependent. Therefore, the capacity of the first cycle at room temperature was defined as 100% for all cells to calculate the relative capacities of the subsequent cycles. A comparison of the losses during formation and the first cycle at room temperature is given in Table 1. The same behavior was observed when both the first formation cycle and a second subsequent cycle were conducted at other temperatures than 25 °C and room temperature was applied in the third cycle (not shown here). The increase of losses with temperature could be due to decomposition reactions of the electrolyte components at elevated temperature. The incomplete "recovery" of the losses in the first cycle at room temperature after a formation at 15 °C will be discussed later. The decrease of capacity during cycling may have various reasons which lead to an increase of the inner resistivity like structural changes, micro-cracking or loss of contact due to mechanical stress, or decomposition reactions. The improved cyclability with increased formation temperature could be explained by competing processes: the increased temperature enhances electrochemical processes and reduces resistivities, whereas the calendar aging is accelerated as well.

Obviously, the capacity retention of the graphite negative electrode decreases with increasing formation temperature. This decrease is due to an increase of the interface resistivity of the graphite electrode caused by the growth of the SEI layer. As mentioned before, structural defects within the SEI are suggested to increase with formation temperature. This leads to an increase of electrolyte reduction during cycling. [8] The reduced protection of the graphite by the SEI may also be reflected in the first cycle at room temperature where the losses slightly increase with formation temperature (Table 1).

In summary, full cell's aging through cycling is apparently dominated by the influence of the graphite negative electrode. Such an increase of the formation temperature leads to an increased capacity fading for both full cells and graphite half cells.

**Table 1**
The capacity losses of half cells for (a) formation at the temperature stated, and (b) a subsequent cycle at room temperature, respectively. The losses are calculated via the absolute loss [Ah] with respect to 100% state-of-charge [Ah] received from the first formation charge.

| $T$/°C | Capacity loss (a)/% | | Capacity loss (b)/% | | Total capacity loss/% | |
|---|---|---|---|---|---|---|
| | NCM | Graphite | NCM | Graphite | NCM | Graphite |
| 15 | 26.4 | 9.5 | −3.9 | 0.2 | 22.5 | 9.7 |
| 25 | 19.7 | 9.9 | −0.6 | 0.5 | 19.1 | 10.4 |
| 35 | 17.2 | 10.8 | 5.1 | 0.6 | 22.3 | 11.4 |
| 45 | 15.0 | 13.3 | 8.5 | 0.8 | 23.5 | 14.1 |

### 3.3. Analysis of the formation losses

#### 3.3.1. Effect of temperature

The decrease of capacity losses for NCM with temperature and the subsequent approximation at room temperature indicate a kinetic effect. For this reason a forced discharge after initial charge of an NCM half-cell was carried out at 25 °C until the discharge capacity was equal to the charge capacity. The result is shown in Fig. 3a (solid curve). An additional plateau occurs at a potential around 1.4 V vs. $Li^+/Li$. This low-voltage plateau is associated with the formation of the overlithiated phase $Li_2(Ni_{1/3}Co_{1/3}Mn_{1/3})O_2$ at the oxide particle surface due to a high activation energy when the lithium concentration $(1-x)$ reaches values close to 1 in $Li_{1-x}(Ni_{1/3}Co_{1/3}Mn_{1/3})O_2$, and diffusion becomes very slow [27–32]. So the sudden voltage drop near 3.6 V and the plateau at around 1.4 V can be attributed to high lithium-ion concentration and two-phase coexistence of $Li_{1-x}(Ni_{1/3}Co_{1/3}Mn_{1/3})O_2$ and $Li_2(Ni_{1/3}Co_{1/3}Mn_{1/3})O_2$, respectively, at the oxide particle surface. Similar behavior has been reported for other lithium metal oxides [28,29,31–36]. Since the overlithiated phase results from a kinetic limitation, it disappears after an extended relaxation time, and the half-cell reaches a value of around 3.3 V again (Fig. 3b, solid curve). Kang et al. [27] proposed a two-step relaxation process with lithium diffusion across the $Li_2(Ni_{1/3}Co_{1/3}Mn_{1/3})O_2$–$Li_{1-x}(Ni_{1/3}Co_{1/3}Mn_{1/3})O_2$ phase boundary what correlates with a phase transition (plateau), and sluggish lithium diffusion within $Li_{1-x}(Ni_{1/3}Co_{1/3}Mn_{1/3})O_2$ afterward.

In a half-cell setup, where a lithium counter electrode and therefore infinite lithium source is used, the possibility of a 100% lithium recovery is given a priori. Thus this procedure was repeated with an NCM full cell loaded with graphite as counter electrode (dotted curve in Fig. 3a). Near the middle of the lower extra plateau another voltage drop occurs. At this point, the entire lithium has been deintercalated from graphite, and copper-dissolution ($Cu \rightarrow Cu^+$) of the current collector begins. It was not examined in what extend NCM was coated by copper, but after a deep discharge to charges $\gg$100% relative to the charge flow the positive electrode was coated with a visible film of copper and the current collector of the negative electrode had disappeared. The fast rise of the voltage without a plateau (Fig. 3b, dotted curve) to 3.39 V vs. $Li^+/Li$ describes the reaction $Cu \rightarrow Cu^{2+} + 2e^-$. This means that the previously deposited copper on the positive electrode dissolves again. The related reductive reaction is probably the lithium intercalation into NCM, resulting in self-discharge.

At the point where copper-dissolution begins the capacity is only limited by the negative electrode whereby it is possible to estimate the capacity loss due to SEI formation. The difference between this point and 100% recovery is the "real" irreversible loss of the lithium-ion cell (ca. 10%). And as the value of the "reversible loss" on the positive electrode is therefore also ca. 10%, the total loss in a full cell can be attributed to SEI formation and kinetic inhibition about one half each.

Thus the ratio of losses on negative and positive electrode in a full cell apparently increases with increased formation temperature (Fig. 1b) as the lithium diffusion coefficient in NCM increases. The increase in diffusion can also be detected from a shift of the sudden potential drop near 3.6 V to higher coulombic efficiencies with temperature. As the decrease of capacity loss already depicts this condition, the additional curves are not shown in Fig. 3a for clarity.

But also the losses of NCM during the first cycle at room temperature when formation occurred at elevated temperature before must be taken into account for the calculation of the irreversible loss. In total, a higher temperature worsens coulombic efficiency on both electrodes graphite and NCM (cf. Table 1).

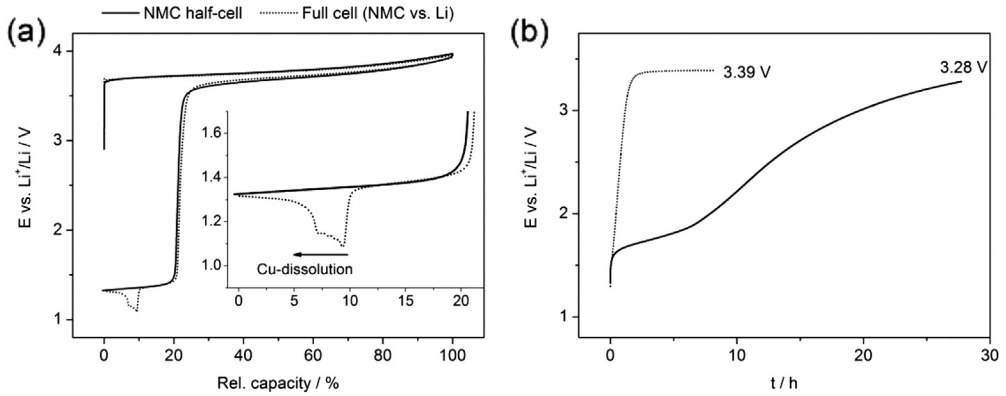


**Fig. 3.** (a) Formation at 25 °C with subsequent deep discharge to 100% coulombic efficiency for an NCM half-cell and an NCM "full cell" (three-electrode test cell with graphite as counter electrode). (b) Relaxation curves after deep discharge to 100% coulombic efficiency after formation.

With these measurements it is possible to explain the effect of lithium loss equalization during the first cycle at room temperature. The incomplete approximation of losses at 25 °C after formation at 15 °C is probably due to an insufficient lithium diffusion coefficient in NCM at 25 °C.

It should be noted that the discussed losses depend on the discharge current and generally increase with the C-rate due to increased polarization. This effect also applies to the low-voltage plateau of NCM which shifts to lower potentials with increasing current and has been observed in own experiments but has also been reported elsewhere [28]. This effect is mainly due to an increase of the ohmic resistivity. But other effects like diffusion and charge transfer over-voltages also have an influence.

### 3.3.2. *Effect of the upper cut-off voltage*

The upper cut-off voltage (UCV) has also an effect on the formation losses. Full cells were charged with C/10 to different potentials and directly discharged. Afterward, a full cycle with an UCV of 4.2 V was added. The corresponding losses are displayed in Fig. 4. Obviously, the formation losses increase within the 1. cycle when upper cut-off voltages of 3.6 or 3.7 V are applied. In the 2. cycle, an almost complete recovery of these losses occurs. An UCV of 3.8 V or higher reveals no differences concerning formation losses. The formation with an UCV of 3.5 V shows decreased losses in the first cycle but a reasonable approximation during a second cycle with an UCV of 3.8 V or higher. This effect can be explained by the fact that intercalation of lithium into graphite mainly occurs at potentials above 3.5 V. The significant decreased losses in total could be assigned to an insufficient SEI formation during the first charge. A further growth or relaxation of the SEI is still expected above 3.5 V.

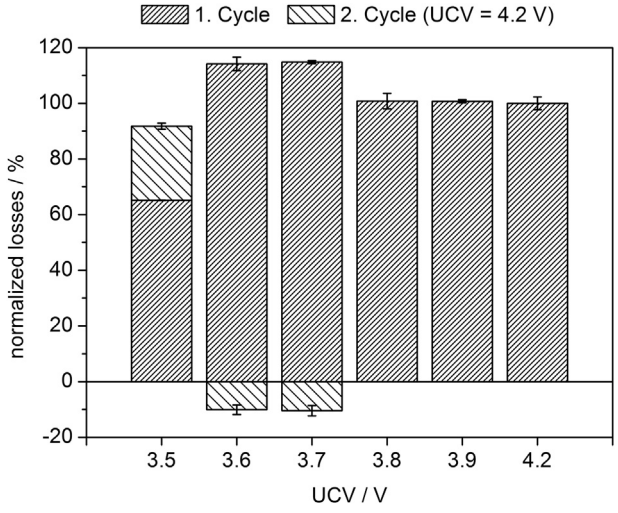


**Fig. 4.** Formation losses (normalized to formation with UCV of 4.2 V) of pouch cells for various upper cut-off voltages. The losses of the second cycle (UCV of 4.2 V) are negligible for voltages above 3.7 V. At least 3 cells were used per test.

To examine the reason of the increased losses in the range of 3.6–3.7 V (what correlates with a state-of-charge (SOC) of about 50%), fresh half cells of graphite and NCM were charged for 5 h with C/10, followed by a direct discharge and subsequent cycles with C/2 charges for 2 h, respectively. The results are shown in Table 2. It can be seen that a small part of the losses in a graphite half-cell were displaced into the second cycle when only charged to 50% in the first run. In total the losses are the same as for the formation to 4.2 V. An uncompleted SEI formation and a further SEI growth above 50% SOC could be an explanation for this effect. NCM shows significantly increased losses when not fully charged but a recovery during subsequent cycles. This could be ascribed to the lithium diffusion in NCM. When the lithium diffusion direction gets inverted within a potential region that possesses a high d$Q$/d$E$-gradient, the two diffusion currents influence each other. The NCM particles are definitely far away from equilibrium when the discharge process begins. So the lithium diffusion from surface to bulk will probably counteract with the deintercalation process and the capacity drop around 3.6 V sets in earlier.

However, the effect noticed in full cells can be related to the NCM positive electrode and is reversible. Further experiments have shown that capacities of full cells charged to only SOC 50% in the first cycle reach similar capacity like cells which underwent a formation to 4.2 V after a few subsequent full cycles. The same effect was observed with NCM half cells.

**Table 2**
The capacity losses (room temperature) for (a) formation with charging step to the state-of-charge (SOC) stated, and (b) a subsequent cycle with charging step to 100% SOC, respectively. The losses are calculated via the absolute loss [Ah] with respect to 100% state-of-charge [Ah] received from the first formation charge.

| SOC/% | Capacity loss (a)/% | | Capacity loss (b)/% | | Total capacity loss/% | |
|---|---|---|---|---|---|---|
| | NCM | Graphite | NCM | Graphite | NCM | Graphite |
| 100 | 19.7 | 9.9 | −0.2 | 0.5 | 19.5 | 10.4 |
| 50 | 27.1 | 8.5 | −5.3 | 1.2 | 21.7[a] | 9.7 |

[a] Continuing cycling leads to further recovery and an approximation of capacity with cells underwent formation to 100% SOC in first cycle.

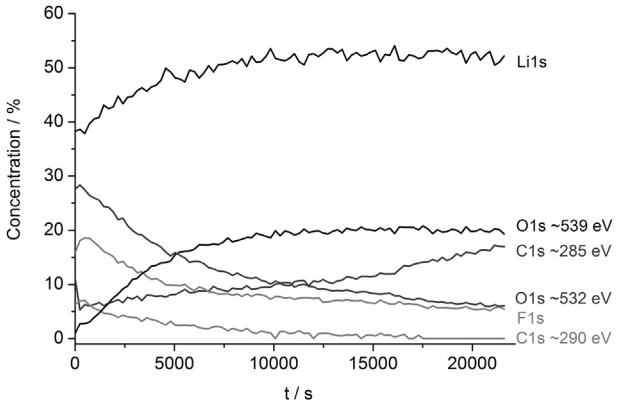


**Fig. 5.** Depth profile of a graphite negative electrode after formation.

### 3.4. SEI characterization

The XPS and FTIR measurements of negative electrodes after formation revealed a high degree of inhomogeneity of the SEI. The concentrations of components even vary between different sample sites on one and the same negative electrode sheet. Therefore it was not possible to explore whether there are any differences in SEI characteristics for different formation procedures. However, increasing the temperature generally means acceleration of reaction but in principle no change of components. For the analysis of possible changes in morphology these methods are apparently not qualified. Nevertheless it was possible to identify the components within the SEI with the combination of these methods.

As mentioned before, the samples were washed with DEC for various times before measurement. Unwashed or short-washed samples showed huge residues of electrolyte and conducting salt on both negative and positive electrode. A washing time of at least 2 h was found to be suitable for the analysis of the outer part of the SEI. An extended washing time leads to dissolution of the organic constituents and the possibility to analyze other depths.

Fig. 5 shows the XPS depth profiling and Fig. 6 the XPS spectra after different DEC washing times. From both methods a different structure of the inner and outer part of SEI can be deduced. The short or long washing times are comparable to short or long sputter times, respectively. The classification of the SEI into an outer organic and an inner inorganic layer as it also reported in Refs. [7,37] can be confirmed.

The outer part consists of $RCH_2OCO_2Li$ and LiF. The presence of ROLi and $Li_2CO_3$ is neither certain nor excluded. The inner layer is dominated by $Li_2CO_3$, LiF (less than in outer layer) and $Li_2O$. The composition of the SEI after the different washing times is displayed in Table 3. Since no fluorine signal from the binder is apparent in the spectra the entire amount of F can be assigned to LiF. The remaining Li belongs mainly to organic constituents in the outer part of the SEI, and to $Li_2CO_3$ and $Li_2O$ in the inner part. The assignments of the binding energies were carried out using [6,37–39].

Of course the formation of $Li_2O$ from $Li_2O_3$ decomposition due to $Ar^+$-sputtering cannot be excluded as it is described elsewhere [6,37]. But the existence of non-artifact $Li_2O$ is sure since the measurements after 16 h washing time clearly evidence the presence of $Li_2O$. Due to overlapping binding energies the presence of LiOH cannot be excluded from the XPS spectra alone, but its absence also in the FTIR spectra indicates the LiOH is indeed not present in the SEI layer of the electrodes.

The FTIR spectrum of the SEI found on the negative electrodes is shown in Fig. 7. $Li_2CO_3$ and $RCH_2OCO_2Li$ from XPS are confirmed, and furthermore RCOOLi is found. It is not possible to identify ROLi

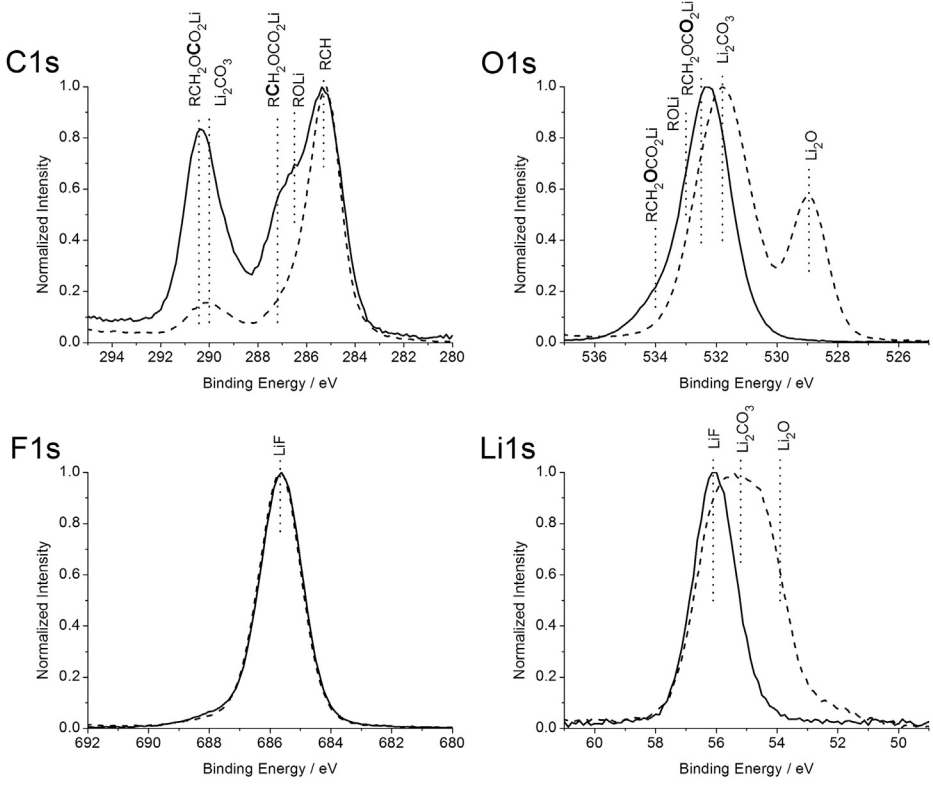


**Fig. 6.** XPS spectra of graphite negative electrodes after formation received after a 2 h (solid line) or 16 h (dashed line) wash with DEC.

**Table 3**
Composition of the SEI on graphite negative electrodes after formation in dependence of the DEC washing time received from XPS measurements.

| Washing time/h | Li1s/% | C1s/% | O1s/% | F1s/% |
|---|---|---|---|---|
| 2 | 34.6 | 22.3 | 22.9 | 20.2 |
| 16 | 43.1 | 21.8 | 22.6 | 12.5 |

unambiguously, even not in combination with XPS. The assignment of the bands was carried out using [40,41].

With varying the washing time the composition of the SEI examined with FTIR does not change, only the intensities of the bands decrease. The presence of $Li_2O$ as well as PVDF on the short-washed samples can be explained by the high information depth compared with XPS.

The Raman spectra of the negative electrodes (washed with DEC for 10 s) for different formation temperatures and a pristine negative electrode as reference are shown in Fig. 8. The intensities of the spectra were normalized to the maximum of the intensities of the G bands (1573 $cm^{-1}$ for the pristine negative electrode). For all formation temperatures the width of the G band increases in comparison to the pristine negative electrode. Furthermore a shift to higher wavenumbers (ca. 1591 $cm^{-1}$) together with a slight splitting is observed. This is due to the formation of lithium layers within the graphite structure. [42,43] The positions of the D bands for both the reference negative electrode and negative electrodes after formation at 45 °C are about the same (ca. 1326 $cm^{-1}$). The broadened band after formation occurs from an increased degree of disorder caused by co-intercalation of solvent molecules. [44] A shift of the D band with decreased formation temperature to lower wavenumbers combined with a change of its shape can be observed. It also seems that the 45 °C formation leads to a less structural disorder as the D band is relatively distinct and the integral ratio of the D and G band (called *R* value, 1.2 for the pristine negative electrode) is smaller than for the other temperatures (1.4 vs. 2.0). The formation at 15 or 25 °C leads to changed electronic properties of graphite as an additional shoulder occurs at around 1555 $cm^{-1}$. This shoulder is assumed to be a so-called Breit–Wigner–Fano (BWF) line. Such lines are caused by metallic character and usually appear in metallic single-walled carbon nanotubes but may also occur in graphite intercalation compounds [45,46].

These significant changes with variation of the formation temperature could be due to a changed surface structure caused by the different SEI formation conditions. The decreased cycling stability of graphite negative electrodes with increased formation temperature indicates that a more effective SEI in terms of surface coverage and adherence is probably formed at lower temperatures. This may also have an influence on the electronic surface structure of graphite as indicated by the appearance of the BFW line. Another possibility for a changed D band shape is an altered ratio of the sub-bands $D_1$ and $D_2$ (wavenumber $D_2 > D_1$). The photo-excited electrons can be first scattered by a phonon ($D_1$) or a defect ($D_2$). [47] After formation the probability of a "defect-first" process is increased. However, for the herein investigated material a distinct separation of these sub-bands is not possible.

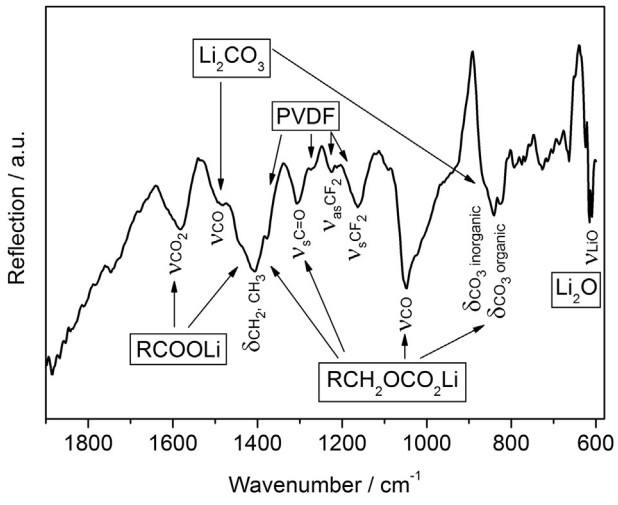


**Fig. 7.** FTIR spectrum of a graphite negative electrode after formation.

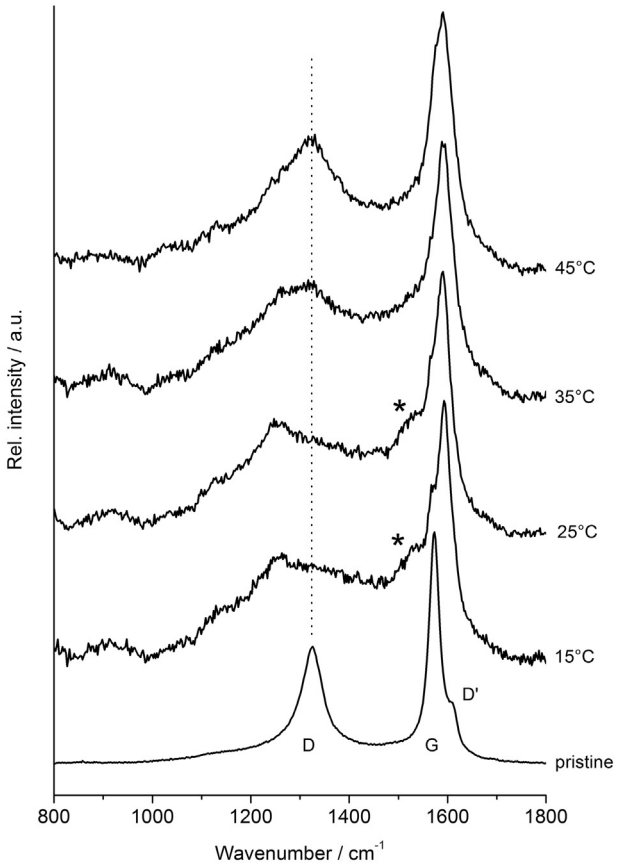


**Fig. 8.** Raman spectra of graphite negative electrodes after formation at different temperatures. As reference a spectrum of a pristine negative electrode with labeled D, G and D′ band is given. (*) After formation at 15 and 25 °C an additional shoulder, assumed to be a BWF line, is present.

The SEI is assembled of an outer mainly organic layer with the demonstrably found species $RCH_2OCO_2Li$, RCOOLi, LiF and possibly ROLi and $Li_2CO_3$, and an inner layer consisting of mainly $Li_2CO_3$, $Li_2O$ and LiF. The increased amount of LiF in the outer layer could be explained by further decomposition of the conducting salt right after the SEI is largely formed.

FTIR of NCM after formation and a 2 h DEC wash shows no differences to a fresh positive electrode. This means no SEI or other film formation occurs on this electrode to a great extent. This is consistent with the electrochemical results.

## 4. Conclusion

With the comparison of NCM- and graphite half cells and full cells it was possible to understand the contributions of both negative and positive electrode on formation losses and cell aging

in full cells. Graphite shows irreversible losses due to SEI formation and NCM mainly reversible losses due to kinetic effects. It could be demonstrated that the lithium loss during the formation of a lithium-ion full cell at 25 °C is attributed to SEI formation and kinetic inhibition about one half each. The aging with the attending increase of the internal resistivity can be mainly assigned to the graphite electrode. It was also shown that with increasing formation temperature the initial losses of graphite increase and that of NCM decrease but appear during the first cycle at room temperature resulting in an increased loss in total. The formation losses in full cells are dominated by "reversible" losses of NCM. With increasing formation temperature the subsequent cycle stability becomes lower for the graphite electrode, but slightly increases for NCM. In a full cell elevated formation temperatures above room temperature are not of advantage since both NCM and graphite show increased losses and the poorer cycle stability of graphite dominates the performance of the full cell. The upper cut-off voltage also has an influence on the formation losses, but only in a reversible manner.

Although the performance of the used test cells and the commercial pouch cells differ tremendously, it is possible to test the individual electrodes in an appropriate way to obtain prospects on their behavior.

With the combination of XPS and FTIR measurements it was possible to identify the constituents of the outer (mainly $RCH_2O$-$CO_2Li$, RCOOLi and LiF) and inner (mainly $Li_2CO_3$, $Li_2O$ and LiF) SEI.

## References


[1] E. Peled, D. Golodnitsky, C. Menachem, D. Bar-Tow, J. Electrochem. Soc. 145 (1998) 3482–3486.
[2] Y. Ein-Eli, Electrochem. Solid-State Lett. 2 (1999) 212–214.
[3] S.-K. Jeong, M. Inaba, T. Abe, Z. Ogumi, J. Electrochem. Soc. 148 (2001) A989–A993.
[4] T. Zheng, A.S. Gozdz, G.G. Amatucci, J. Electrochem. Soc. 146 (1999) 4014–4018.
[5] M. Herstedt, D.P. Abraham, J.B. Kerr, K. Edström, Electrochim. Acta 49 (2004) 5097–5110.
[6] K. Edström, M. Herstedt, D.P. Abraham, J. Power Sources 153 (2006) 380–384.
[7] M. Winter, J.O. Besenhard, M.E. Spahr, P. Novák, Adv. Mater. 10 (1998) 725–763.
[8] S.-B. Lee, S.-I. Pyun, Carbon 40 (2002) 2333–2339.
[9] B. Blizanac, S. Mentus, N. Cvijeticanin, N. Pavlovic, J. Serb. Chem. Soc. 68 (2003) 119–130.
[10] M. Inaba, H. Tomiyasu, A. Tasaka, S.-K. Jeong, Z. Ogumi, Langmuir 20 (2004) 1348–1355.
[11] T.L. Kulova, Russ. J. Electrochem. 40 (2004) 1052–1059.
[12] Y.-B. He, Z.-Y. Tang, Q.-S. Song, H. Xie, Y.-G. Liu, Q. Xu, J. Electrochem. Soc. 155 (2008) A481–A486.
[13] M. Dollé, S. Grugeon, B. Beaudoin, L. Dupont, J.M. Tarascon, J. Power Sources 97–98 (2001) 104–106.
[14] P.-C.J. Chiang, M.-S. Wu, J.-C. Lin, Electrochem. Solid-State Lett. 8 (2005) A423–A427.
[15] D. Goers, M.E. Spahr, A. Leone, W. Märkle, P. Novák, Electrochim. Acta 56 (2011) 3799–3808.
[16] H.-H. Lee, Y.-Y. Wang, C.-C. Wan, M.-H. Yang, H.-C. Wu, D.-T. Shieh, J. Power Sources 134 (2004) 118–123.
[17] G.V. Zhuang, H. Yang, B. Blizanac, P.N. Ross, Electrochem. Solid-State Lett. 8 (2005) A441–A445.
[18] F.-M. Wang, H.-Y. Wang, M.-H. Yu, Y.-J. Hsiao, Y. Tsai, J. Power Sources 196 (2011) 10395–10400.
[19] G. Nazri, R.H. Muller, J.E. Soc, J. Electrochem. Soc. 132 (1985) 2050–2054.
[20] E. Peled, D. Golodnitsky, A. Ulus, V. Yufit, Electrochim. Acta 50 (2004) 391–395.
[21] D. Aurbach, Y. Ein-Eli, A. Zaban, J. Electrochem. Soc. 141 (1994) L1–L3.
[22] H. Yoshida, T. Fukunaga, T. Hazama, M. Terasaki, M. Mizutani, M. Yamachi, J. Power Sources 68 (1997) 311–315.
[23] A.M. Andersson, A. Henningson, H. Siegbahn, U. Jansson, K. Edstro, J. Power Sources 121 (2003) 522–527.
[24] S.H. Kang, D.P. Abraham, A. Xiao, B.L. Lucht, J. Power Sources 175 (2008) 526–532.
[25] K. Kim, D. Kam, C.C. Nguyen, S.W. Song, R. Kostecki, Bull. Kor. Chem. Soc. 32 (2011) 2571–2576.
[26] J. Choi, A. Manthiram, Electrochem. Solid-State Lett. 8 (2005) C102–C105.
[27] S.-H. Kang, D.P. Abraham, W.-S. Yoon, K.-W. Nam, X.-Q. Yang, Electrochim. Acta 54 (2008) 684–689.
[28] S.-H. Kang, W.-S. Yoon, K.-W. Nam, X.-Q. Yang, D.P. Abraham, J. Mater. Sci. 43 (2008) 4701–4706.
[29] J.R. Mueller-Neuhaus, R.A. Dunlap, J.R. Dahn, J. Electrochem. Soc. 147 (2000) 3598–3605.
[30] A. Van der Ven, G. Ceder, J. Power Sources 97–98 (2001) 529–531.
[31] C.S. Johnson, J.-S. Kim, A.J. Kropf, A.J. Kahaian, J.T. Vaughey, L.M.L. Fransson, K. Edström, M.M. Thackeray, Chem. Mater. 15 (2003) 2313–2322.
[32] S.-H. Kang, S.-H. Park, C.S. Johnson, K. Amine, J. Electrochem. Soc. 154 (2007) A268–A274.
[33] J.R. Dahn, U. von Sacken, C.A. Michal, Solid State Ionics 44 (1990) 87–97.
[34] S.S. Zhang, K. Xu, T.R. Jow, Electrochem. Solid-State Lett. 5 (2002) A92–A94.
[35] N.K. Karan, D.P. Abraham, M. Balasubramanian, M.M. Furczon, R. Thomas, R.S. Katiyar, J. Electrochem. Soc. 156 (2009) A553–A562.
[36] N. Yabuuchi, K. Yamamoto, K. Yoshii, I. Nakai, T. Nishizawa, A. Omaru, T. Toyooka, S. Komaba, J. Electrochem. Soc. 160 (2013) A39–A45.
[37] A.M. Andersson, A. Henningson, H. Siegbahn, U. Jansson, K. Edström, J. Power Sources 121 (2003) 522–527.
[38] L. Zhao, I. Watanabe, T. Doi, S. Okada, J.-i. Yamaki, J. Power Sources 161 (2006) 1275–1280.
[39] V. Eshkenazi, E. Peled, L. Burstein, D. Golodnitsky, Solid State Ionics 170 (2004) 83–91.
[40] D. Aurbach, Y. Gofer, J. Langzam, J. Electrochem. Soc. 136 (1989) 3198–3205.
[41] P. Verma, P. Maire, P. Novák, Electrochim. Acta 55 (2010) 6332–6341.
[42] S. Migge, G. Sandmann, D. Rahner, H. Dietz, W. Plieth, J. Solid State Electrochem. 9 (2005) 132–137.
[43] M. Inaba, H. Yoshida, Z. Ogumi, T. Abe, Y. Mizutani, M. Asano, J. Electrochem. Soc. 142 (1995) 20–26.
[44] R. Kostecki, F. McLarnon, J. Power Sources 119–121 (2003) 550–554.
[45] M.S. Dresselhaus, G. Dresselhaus, R. Saito, A. Jorio, Phys. Rep. 409 (2005) 47–99.
[46] S.Y. Leung, M.S. Dresselhaus, G. Dresselhaus, Phys. B+C 105 (1981) 375–380.
[47] Z. Luo, C. Cong, J. Zhang, Q. Xiong, T. Yu, Carbon 50 (2012) 4252–4258.